

# 3D meso-structural analysis of concrete specimens under uniaxial tension

A. Caballero, C.M. López & I. Carol  
*ETSECCPB, UPC, Barcelona, SPAIN.*

**ABSTRACT:** This paper describes an approach for the 3-D meso-structural analysis of concrete specimens, which extends the previous work within the same group in 2-D. Concrete is represented as a particle array (larger aggregates), embedded in a matrix (mortar plus smaller aggregates), all discretized using finite elements. Zero-thickness interface elements are inserted along all particle-matrix and selected matrix-matrix element boundaries, to represent the main potential crack planes. Continuum elements are assumed elastic, while the interfaces are equipped with a fracture-based constitutive law to represent cracks. For the 3-D calculations, major efforts are required for mesh generation, improvement of code efficiency and post-processing. As the first application example, a simple uniaxial tension specimen is presented which reproduces the essential experimental features observed, both at the meso- and overall stress-strain levels.

## 1 INTRODUCTION

A numerical approach for the meso-mechanical analysis of heterogeneous materials using zero-thickness join/interface elements with constitutive laws based on non-linear fracture mechanics, has been developed at ETSECCPB (School of Civil Engineering)–UPC in recent years. The results obtained for concrete in 2-D successfully reproduced experimental behavior under a number of load situations, such as uniaxial tension, uniaxial compression, biaxial tension/compression, Brazilian test, creep, shrinkage, etc. [1,2].

For all these loading cases, outstanding results have been obtained in terms of cracking patterns, localization process happening in a “spontaneous” manner, average stress-strain specimen curves, material failure mechanisms, etc. However, the two-dimensional analysis is intrinsically limited. There are many loading cases which cannot be simulated in 2-D (for instance biaxial loading cases which fail out of plane, or triaxial tests), and even for those which can, it would be important to evaluate the importance of the “three-dimensional effect” since, strictly speaking, 2-D calculations would correspond to an arrangement of prismatic aggregates in the third dimension. In this paper, the on-going work for the 3-D extension of this

approach is described, together with the first results obtained for a uniaxial tension specimen.

## 2 MESO-STRUCTURAL GEOMETRY, MESH

### 2.1 General

The approach is based on a polyhedron representation of the larger aggregate pieces, which are embedded in a matrix phase representing mortar plus the smaller aggregates. The polyhedral geometry is numerically generated by standard Voronoi/Delaunay tessellation from a regular array of points which is slightly perturbed [3]. The polyhedra are then shrunk to become the aggregate particles, and both the particles and the space between them (matrix) are meshed with finite elements for the analysis. The main peculiarity of the approach used is that the continuum elements thus obtained are all assumed to behave linear elastic. The non-linearity and failure capability of the model is achieved by means of zero-thickness interface elements equipped with a non-linear fracture-based law, which are inserted between all particle-matrix interfaces and also along selected matrix-matrix inter-element boundaries representing the main potential crack patterns. This obviously restricts failure planes and mechanisms to the planes with interfaces inserted originally in

the mesh, which in turn places strong requirements on the discretization process.

In 3-D, the development of such mesh generator represents significant additional difficulties due to the generation process itself, and to the difficulties for the graphic representation and verification of the resulting meshes.

The overall generation process may be decomposed into two steps: (i) the generation of the basic geometry of the composite material, and (ii) the process of finite element meshing of that geometry. These steps are described in the following subsections.

## 2.2 Aggregate arrangement and geometry.

First, a regular distribution of points is generated in space (Fig. 1a). The type of distribution of initial points significantly conditions the topology and geometry of the resulting Voronoï polyhedra [4,5,3]. The most common distributions are the *Regular Distribution*, the BCC (*Body Centered Cube*), and the FCC (*Face Centered Cube*). Although *a priori* the *Regular Distribution* could seem the simplest arrangement and a good first choice, after slight perturbation the resulting polyhedrons have the tendency to exhibit some very small edges/faces. These tend to zero length/area for vanishing distortion of the initial arrangement, which is an undesirable feature. Both the BCC and FCC are free from this “singular” behavior at no distortion, although in general they also generate some small edges/faces when distortion is introduced. Among them, the BCC distribution has been initially adopted in this work, due to considerations on the adequacy of the resulting geometries for fracture patterns. Once the initial distribution of points has been generated, their position is perturbed by means of a random function. In Fig.1a, an orthogonal projection of a regular distribution of points is shown, and also their perturbed position in figure 1b.

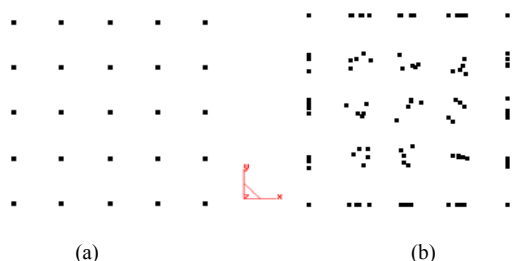


Fig. 1. Lateral view along  $z$ -axis of seed points in: (a) initial regular 3D positions and (b) randomly perturbed positions.

On the perturbed point arrangement, a mesh of Delaunay tetrahedrons is generated following Watson/Lawson's algorithm [6]. A result of this process is shown in figure 2.

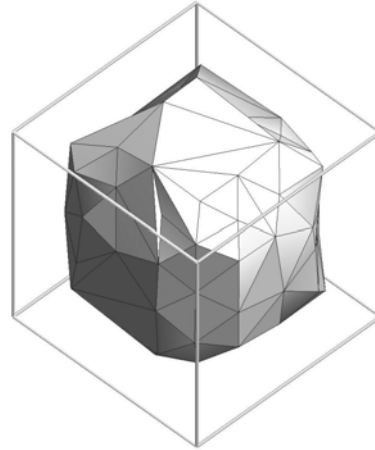


Fig. 2. Delaunay mesh obtained from the perturbed distribution of points in Fig. 2b.

Due to the duality between the Delaunay and Voronoï spaces, once the Delaunay mesh is finished also the Voronoï polyhedrons may be uniquely obtained by connecting the circum-centers of the every Delaunay tetrahedron to all its neighbors with which it shares a triangular face. In a third step, each polyhedron is shrunk by a factor, which can be the same or different for each polyhedron. In addition, and with the purpose of avoiding an excessive alignment of the final polyhedrons, their position may be altered by means of a small solid-rigid movement. A final distribution of  $3 \times 3 \times 3$  BCC Voronoï polyhedrons is shown in Fig. 3, which is represented inside some enlarged outer box, for easier spatial visualization.

Once the polyhedrons generated, shrunk and repositioned, we proceed to fill up the space between them with the matrix, as shown in Fig. 4. To do this, the following properties of Voronoï/Delaunay tessellation are taken into account [5]:

- The opposite faces between two different polyhedrons have the same number of edges and they are parallel to each other, hence they define a prism with a known number of sides.
- The polyhedron edges which were the same before shrinking, define a right prism of triangular base.
- The polyhedron vertices which were the same before shrinking, define a tetrahedron.

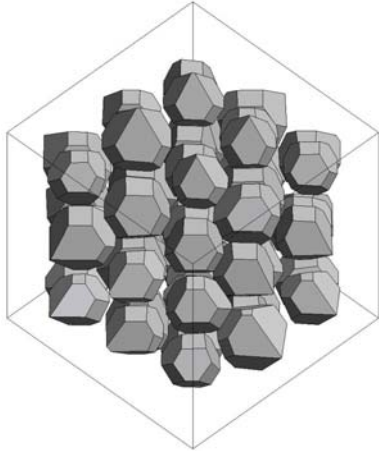


Fig. 3. Resulting Voronoi polyhedrons for a 3x3x3-aggregate example, represented within an enlarged outer box for better visualization.

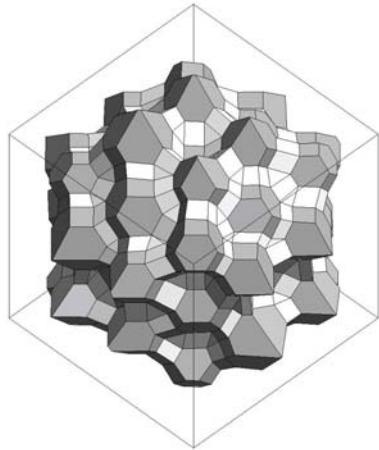


Figure 4. Same geometry as in Fig.3, with the matrix filling the space between shrunk polyhedrons, represented within an enlarged outer box for better visualization.

Once the aggregate geometry is fixed, it is necessary to modify the specimen boundary so that its faces are planes. This part of the generation process turns out to be quite important and relatively complex. The approach followed consists of generating aggregates beyond the specimen boundaries and then cutting them along the side planes, as shown in Fig.5 for the same aggregate geometry of Fig.4 (note that, for easier visualization, the outer box size in previous figures was larger than the actual specimen size). The cutting process modifies the topology of the outer polyhedrons, causing in some cases singularities such as extremely short edges, surfaces with very small angles and excessively flat volumes. These undesirable geometric features are corrected later on in a process that we call “geometry collapse”.

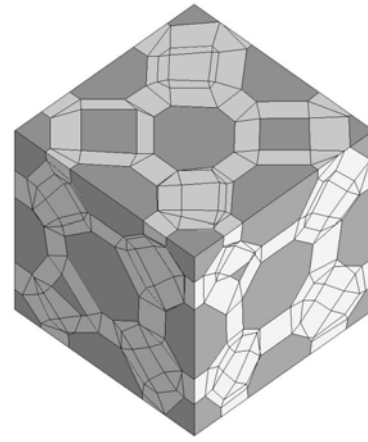


Fig.5. Initial specimen geometry after boundary “cutting” process.

The following step is to insert the interface planes along all potential fracture surfaces to be considered in the analysis. As it is known, in conventional concrete, cracks are initiated mostly along the weaker aggregate-mortar interface, and then propagate within the mortar itself following some path with minimum dissipated energy. At the time of meshing into finite elements, zero-thickness interface elements will be inserted along all these potential fracture surfaces. In order to allow that, all those planes need to be included at this stage as element subdivisions. Aggregate-mortar boundaries are already automatically included in the mesh. Matrix-matrix potential fracture surfaces are included as additional subdivisions of the initial matrix blocks, according to the following criteria:

- a) New subdivisions along planes that are defined by two parallel edges belonging to two opposite polyhedron faces.
- b) New subdivisions along planes that are defined by means of each polyhedron edge and a point located in the center of the space between two polyhedrons facing each other.

This subdivision may produce new “chip” or excessively distorted elements, which in general are also corrected with the “geometry collapse” step. During this step, some points may be slightly repositioned or two or more points collapsed into a single point. If performed directly on the polyhedral geometry of Fig.5, this could cause some polyhedron faces to cease being planes, or some polyhedrons to undergo a partial volume loss. To avoid these situations the whole geometry is first subdivided into tetrahedrons, so that all faces are composed of triangles before the geometry collapse process is applied. In Fig. 6, the geometry

was obtained after inserting the potential fracture surfaces, subdividing into tetrahedrons and applying the collapse process, to the same example of Figs. 4, 5 and 6. Obviously, the final result depends on the allowed tolerances; in this case all the edges with smaller sizes than 20% of the average edge length have been eliminated.

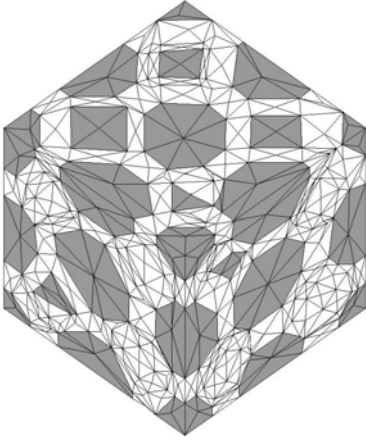


Fig. 6. Final specimen geometry after potential fracture plane insertion, tetrahedron subdivision and collapse process.

### 2.3 FE discretization.

Since at this stage the geometry is already subdivided in tetrahedrons, the simplest discretization may be obtained by simply turning each tetrahedron into a finite element. However, this in general leads to meshes which are too coarse for the analysis, and therefore a further mesh refinement is needed. For this purpose, two procedures have been devised. The first of them, already implemented, is based on structured meshing techniques and simply consists of subdividing each tetrahedron edge into a given number of segments, and the subsequent subdivision of element sides and volumes. A second more sophisticated unstructured meshing technique based on advancing front which would ensure more regular sizes and shapes of the resulting mesh, is under development.

Once the specimen discretization in continuum elements is completed, the interface elements need to be introduced along all potential fracture surfaces. This process consists basically on an orderly duplication of the nodes and subsequent changes in element nodal connectivities. This process increases the number of nodes considerably while the number of continuum elements remains unchanged.

## 3 INTERFACE CONSTITUTIVE LAW

The 3D constitutive law is an extension of the 2D formulation used in previous works [7,8,9,10]. In a local orthogonal reference system, the behavior of the joints is formulated in terms of one normal and two tangential traction components on the plane of the joint,  $\sigma = [\sigma_N, \sigma_{T1}, \sigma_{T2}]^t$  and the corresponding relative displacements  $u = [u_N, u_{T1}, u_{T2}]^t$ , as shown in figure 7.

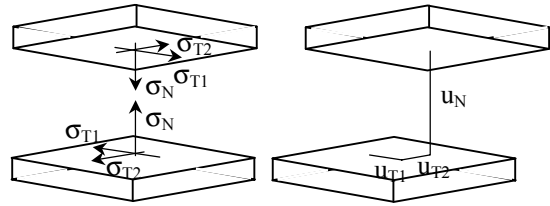


Figure 7. Definition of stress variables and conjugate "strain" variables (relative displacements) for the interface.

The constitutive formulation conforms to work-softening elasto-plasticity, in which plastic relative displacements can be identified with crack openings. The initial loading (failure) surface  $F = 0$  is given as three-parameter hyperboloid (tensile strength  $\chi$ , asymptotic "cohesion"  $c$ , and asymptotic friction angle  $\tan\phi$ ). When cracking starts, the loading surface begins to shrink. This is achieved by means of softening laws in which the surface parameters are functions of the work consumed in fracture processes,  $W_{cr}$ . To control the process of evolution of  $F$ , the model has two parameters that represent the classic energy of fracture in Mode I,  $G_F^I$  (pure tension) and a second energy under "Mode IIa" defined under shear and high compression without dilatancy,  $G_F^{IIa}$ , with values generally higher than its mode I counterpart. Under pure tension the loading surface shrinks and moves to become another hyperboloid with vertex at the coordinate origin. Under mixed-mode, it degenerates further, asymptotically becoming a cone that represents the residual friction after all roughness of the crack surface has been eliminated. The model is associated in tension  $F = Q$ . In compression, behavior is non-associated, with a reduction of dilatancy which is higher with the joint degradation level and with the evolution of joint degradation measured by apparent cohesion  $c$ . More details of the interface law and examples of application to simple loading cases in 2-D can be found in [8,9,1].

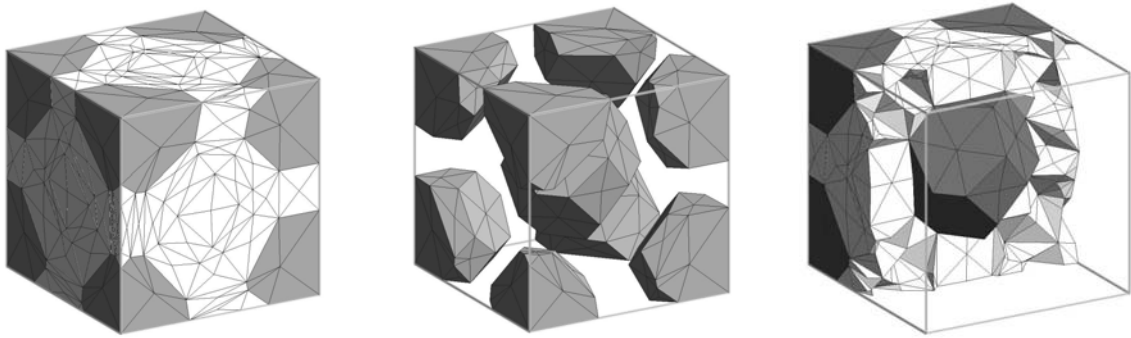


Fig. 8. FE mesh used in application example: (a) external view, (b) aggregates only and (c) partial view of the mesh showing clearly the central aggregate in specimen .

#### 4 COMPUTATIONAL ASPECTS AND PRELIMINARY RESULTS

Moving from 2D to 3D calculations represents a very serious computational challenge because of the dramatic increase of the resources needed at every step of the process. In particular, the number of degrees of freedom involved, which in a typical 2D calculation with 6x6 aggregates including interfaces was in the order of a few thousands, easily reaches a hundred thousand with the 3x3x3 aggregate meshes represented in figures 3-6. And the computational time increases quadratically with the number of d.o.fs.

This is why the specimen considered for the preliminary calculations presented in this section is the simplest possible which could be still considered in a broad sense representative of the overall concrete behavior. As shown in Fig. 8, this specimen contains nine aggregates, eight in its corners, and one in the center. Even if very simple, the resulting mesh with interfaces has 32406 d.o.fs, with 3133 tetrahedrons and 5187 interface elements. Still, the computer code DRAC used for these calculations, has required a number of improvements including a new iterative solver which is much more efficient for large systems. With these improvements, a single elastic solution of the 9-aggregate example takes 12.5 seconds on a PC machine equipped with a P4 1.8GHz processor, 1Gb RAM and running under Windows XP.

The material parameters used are:  $E = 70000$  MPa (aggregate),  $E = 25000$  MPa (mortar) and  $\nu = 0.20$  (both) for the continuum elements; for the aggregate-mortar interfaces:  $K_N = K_T = 10^9$  MPa/m,  $\tan\phi_0 = \tan\phi_r = 0.8$ , tensile strength  $\chi_0 = 3$  MPa,  $c_0 = 10.0$  MPa,  $G_f^I = 0.03$  N/mm,  $G_f^{IIa} = 10$   $G_f^I$ ,  $\sigma^{dII} = 7$  MPa, and all other parameters equal to zero; for the mortar-mortar interfaces the

same parameters except for  $\chi_0 = 6$  MPa,  $c_0 = 20.0$  MPa,  $G_f^I = 0.06$  N/mm.

A prescribed tensile displacement is applied to the upper side of the specimen, while the lower side is fixed vertically. Lateral displacements are left free, except for two nodes at the base of specimen to prevent rigid-body motion/rotation. The resulting average stress-strain curve is represented in Fig. 9, in which average strain is calculated as the prescribed displacement divided by specimen length, and average strain as the sum of reactions (on either upper or lower specimen sides), divided by the side area surface.

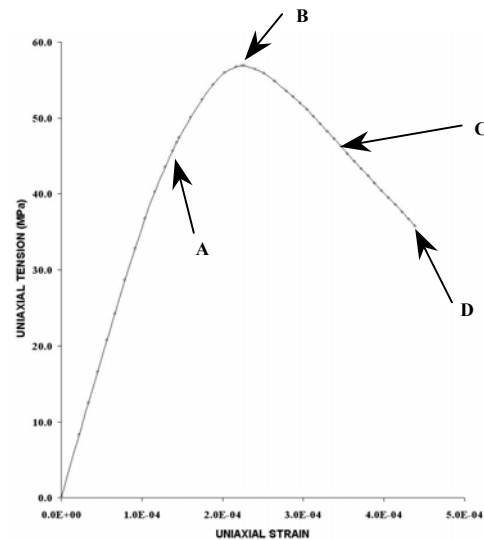


Fig.9. Average stress-strain curve for application example, with loading states A,B,C,D indicated for reference in Fig. 10.

The sequence of cracking and deformed mesh states for loading states A,B,C,D indicated in Fig. 9, are represented in Fig. 10.

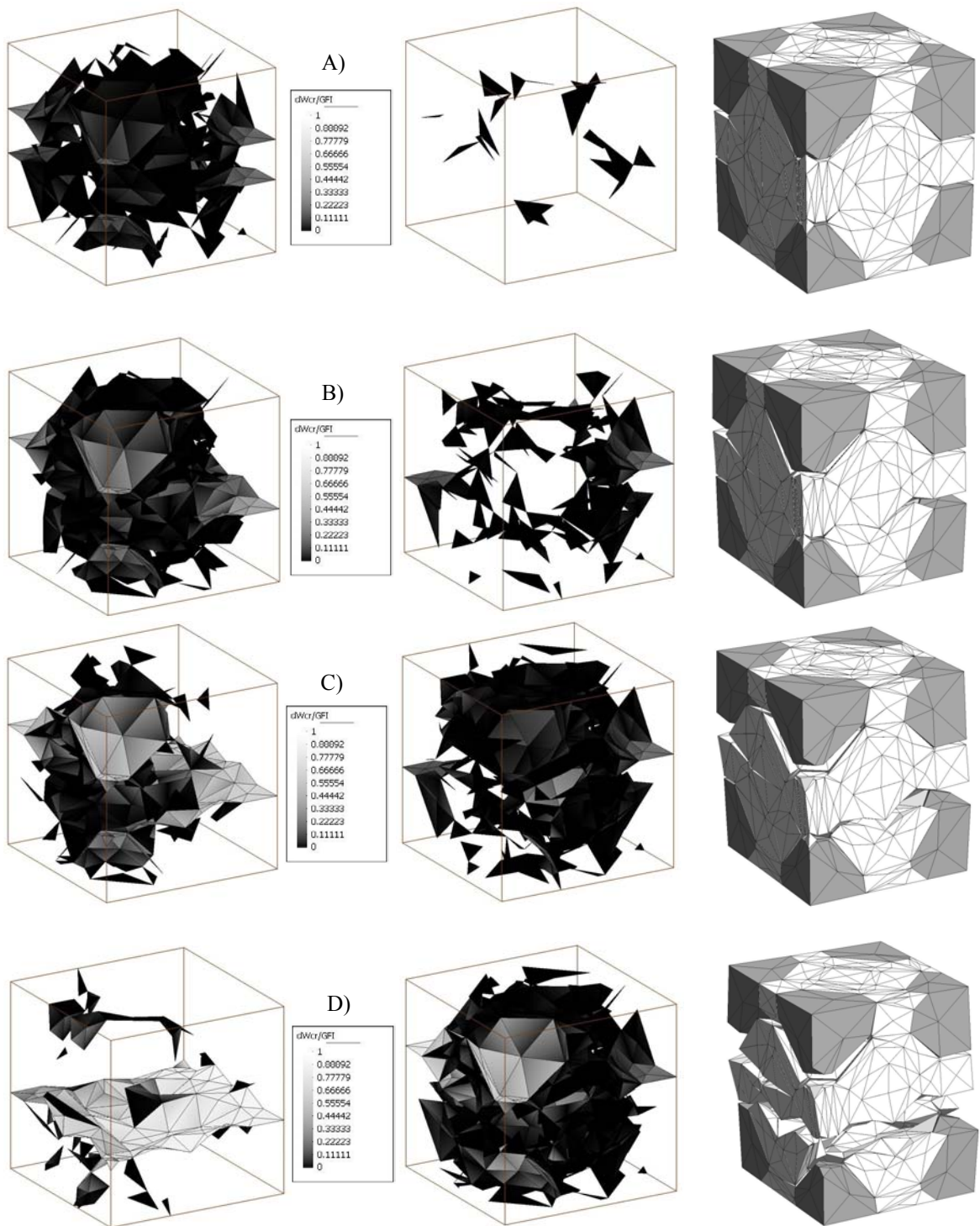


Figure 10. History parameter  $W_{cr}/G_F^I$  on cracked interfaces which are opening (left column), closing (center column) and deformed shape of specimen, at loading states A, B, C and D.

The four images in the right vertical column of Fig.10 represent the deformed shape of the specimen at loading stages A, B, C and D in the stress-strain diagram of Fig. 9. The images in the left and center columns of the figure depict the interfaces which have exceeded the initial strength and therefore have started to open, with different color intensities depending on the amount of energy dissipated in fracture,  $W^{cf}$ . Among them, the left column includes those interfaces which are opening (“plastic loading” state in the constitutive equation), while the central column includes those which are arrested (“elastic unloading”).

In the figure, it can be clearly seen that initially (loading stage A) cracked interfaces are spread more or less uniformly over the specimen and are practically all in “loading” state. Progressively (rows B and C), fracture advances faster in some interfaces, while more and more other interfaces start unloading. Finally (row D), practically only one single surface remains active, which represents the final macrocrack splitting the specimen in two pieces just above the four lower aggregates, while all the other cracks are arrested. Note especially the competing crack which develops until load stage C just below the upper corner aggregate in the front of the image, which finally also arrests at stage D. Note also the complexity of crack patterns which emerge from this simple geometry, with profuse spatial bridging and branching until the final failure mechanisms are defined.

## 5 CONCLUDING REMARKS

The approach for concrete fracture using interface elements previously developed in 2-D, is being successfully extended to 3-D. This extension is requiring an important effort for improving efficiency of the pre-processing, analysis and post-processing tools. The first case analyzed which is described in this paper, represents the simplest meso-geometry with 9 aggregates and also the simplest loading situation –uniaxial tension. In spite of that, a realistic representation of the stress-strain curve and of the crack patterns and evolution are obtained. In particular, it is reassuring to see how the localization process takes place spontaneously, leading from initially distributed micro-cracking to a single macro-crack which crosses the specimen perpendicular to the applied load. Current work aims at the analysis of more representative geometries with larger number of

aggregates, subject to uniaxial tension and compression, as well as more complex loading situations, all of which is linked to on-going parallel developments on the corresponding computational tools.

## 6 ACKNOWLEDGEMENTS

The first author wants to thank MECD (Madrid) for his “FPU” doctoral fellowship. The second author thanks MCYT (Madrid) for his position funded under the “Ramón y Cajal” program. The research grant MAT2000-1007 also from MCYT is also gratefully acknowledged.

## 7 REFERENCES

- [1] Carol, I., López C. M. y Roa, O., “Micromechanical analysis of quasi-brittle materials using fracture-based interface elements”, *Int. J. Numer. Meth. in Engrg.* Vol 52, pp.193-215 (2001).
- [2] López, C., Carol, I., Aguado, A., “Microstructural analysis of concrete fracture using interface elements”, *ECCOMAS2000, Barcelona, Spain, CIMNE* (2002).
- [3] Klein, Rolf “Concrete and abstract Voronoï diagrams”, Springer-Verlag (1989).
- [4] Okabe, A., Boots, B., Sugihara, K., “Spatial tessellations: concepts and applications of Voronoi diagrams”, John Wiley & Sons (1992).
- [5] Hernández, F., “3D mesh generation based on Voronoi diagrams”, (in spanish) Masters thesis, ETSECCPB, Universidad Politècnica de Catalunya, Barcelona, Spain (1998).
- [6] Milind, N., ”Mesh Generation for FEM”. M.Tech. Dissertation, Indian Institute of Technology - Bombay, Department of Civil Engineering, April 1995.
- [7] Carol, I. y Prat, P.C., “A statically constrained microplane for the smeared analysis of concrete cracking”. In Bicanic and Mang, editors, *Computer aided analysis and design of concrete structures*, 919-930, Balkema (1990).
- [8] Carol, I., Prat, P. C. y López, C. M., “A normal/shear cracking model. Application to discrete crack analysis”, *J. of Engineering Mechanics*, 123, No 8, pp. 765-773 (1997).
- [9] López, C. M., “Microstructural analysis of concrete fracture using interface elements. Application to various concretes”. Doctoral Thesis (In Spanish). ETSECCPB, Universitat Politècnica de Catalunya, Barcelona, Spain (1999).